On the Role of Classical Field Time Correlations in Noisy Light Spectroscopy: Color Locking and a Spectral Filter Analogy†

Darin J. Ulness

Department of Chemistry, Concordia College, Moorhead, Minnesota 56562

Received: October 17, 2002; In Final Form: March 7, 2003

Physical concepts which have proven to be of substantial aid in the understanding of the underlying physical mechanisms of noisy light spectroscopy are established and discussed. These physical concepts are extracted from the technique of factorized time correlation diagram analysis. Examples are presented to add concreteness the general discussions of the physical concepts with coherent anti-Stokes Raman scattering of noisy light serving as a particularly useful example.

I. Introduction

It is truly a honor to contribute to this special issue memorializing Professor A. C. Albrecht. As is clear from his numerous contributions to the literature, Professor Albrecht was an excellent and leading scholar. What might be less evident, however, is Professor Albrecht's contribution to science as a teacher. As his many students, which includes the present author, will surely verify, Professor Albrecht was truly a remarkably gifted teacher. He was a patient and kind mentor who gave his students a great gift as he molded them into scientists. His recent passing is a tremendous loss to the scientific community: he will be deeply missed.

This special issue will no doubt cover many of the areas of physical chemistry in which Professor Albrecht has contributed. The current paper deals with one of those areas: noisy light spectroscopy.[1−53] Professor Albrecht was one of the leaders of this interesting field from very early in its development to the present time, with most of his efforts coming from 1986−2001. Professor Albrecht published 30 papers and gave numerous talks on the subject of noisy light spectroscopy.

It has long been known that broadband nontransform-limited quasi-continuous wave noisy light (hereafter referred to simply as noisy light) can be used to achieve femtosecond scale interferometric time resolution.[1−3] The main idea in the use of noisy light for ultrashort timing is that, as opposed to the use of coherent short (femtosecond) pulses, it is the coherence (or correlation) time τ_c of the light, not the temporal profile of its pulse, that determines the time resolution. In principle, the noisy beam may be continuous wave (cw), although in practice it is often pulsed on the ordered of nanoseconds (still essentially cw relative to femtosecond and picosecond material dynamics). The coherence time of the light produced by standard laser dyes operating in a broadband laser (such that much of the emission spectrum of a given dye is released) is typically on the scale of hundreds of femtoseconds, proportional to the reciprocal bandwidth Γ of the noisy light spectrum $J(\omega)$. In a typical experiment, the noisy source enters a dispersion-compensated Michelson interferometer to generate identical twin beams. One of the beams (referred to as B′ and having wavevector $\mathbf{k}'$) is delayed by time τ over the other (referred to a B and having wavevector $\mathbf{k}$) by use of a controllable spatial delay in one of the arms of the interferometer.

Noisy light can be used to probe molecular dynamics, and it offers an unique alternative to the more conventional frequency domain (narrow bandwidth) spectroscopies and ultrashort (femtosecond scale) pulse time domain spectroscopies. Like the frequency domain spectroscopies, the cw nature of noisy light allows precise measurement of transition frequencies. However, like time-resolved techniques, its ultrashort noise correlation time offers the time resolution to directly measure the time domain material response. There is a noisy light analogue for nearly every current conventional optical spectroscopy. Notable exceptions are those spectroscopies that explicitly exploit the phase-locked nature of short pulses. In short, noisy light techniques offer a third means of studying molecular line shapes which complements the more familiar cw and ultrashort pulse techniques.

The differences in these three techniques are apparent in the excitation source. Continuous wave experiments involve the use of beams which have a very narrow spectral bandwidth. In fact, in nearly all cases, a perfectly coherent monochromatic source can be assumed without introduction of any significant error into the theory. The monochromatic nature of this type of excitation source makes it ideal for directly probing spectral features of the sample. The disadvantage is that all the time resolution is lost: no direct time measurements can be made. Time information must be obtained through analysis of the spectral information (i.e., through Fourier transformation of the experimental data). Short pulse experiments are in sharp contrast to cw experiments because, because in short-pulse experiment, many frequencies are present in the spectrum of the excitation light source. In order for these frequency components to conspire to produce a short pulse, they must be *phase-locked* (not to be confused with phase matching). That is, all frequency components must be have a precise phase relationship with one another. The short pulses are ideally suited for direct time measurements. The downside to this is that (finely resolved) spectral information must be determined through analysis of the time information. The phase-locked requirement forces a loss in the ability to directly probe the sample spectrally. (Gross spectral probing is possible since real short pulses do not have infinitely broad spectra.) Spectral information often appears as quantum beats which can be quite complicated if many oscillations are present.

† Part of the special issue "A. C. Albrecht Memorial Issue".

10.1021/jp0222494 CCC: $25.00
Published on Web 05/17/2003

Noisy light has a similar spectrum to that of short pulses, with the important distinction that it is completely *phase-unlocked*. That is, the phase of each frequency component is completely independent of any other component. In a sense, each frequency component is behaving as if it came from an independent cw source. In other words, the noisy light is built from an incoherent superposition of monochromatic cw light. This random superposition produces a beam that carries an electric field, which is a stochastic function of time. One says the noisy light is *color-locked*, because each color (or frequency) is coherent only with itself: it is uncorrelated with any other color. The color locking gives noisy light the ability to probe fine spectral features more directly than with short pulses (each quantum state is probed independently rather than coherently) and probe time features more directly than cw beams. The disadvantage is that neither frequency nor time features can be directly probed without some data analysis. So, in some sense, noisy light is an intermediate between cw and short-pulse methods.

Experimentally, the difficulties inherent with noisy light techniques are on par with cw methods. These techniques are significantly easier to setup and perform than ultrashort pulse techniques. One main reason for this is that optical dispersion has very little effect on noisy light techniques, and it is quite easily controlled in the experimental setup.[14] Second, no sophisticated pulse generation or amplification is needed. From a pragmatic point of view, noisy light and cw experiments are generally less expensive and their signals are strong and quite robust relative to the short-pulse case.

The theory describing noisy light spectroscopy is necessarily more complicated then its conventional (noise-free) counterparts because appropriate treatment of the noise correlations must be superimposed on the conventional theoretical description. A diagrammatic approach called factorized time correlation (FTC) diagram analysis, invented and developed by Professor Albrecht's group, has aided the theoretical investigation of noisy light spectroscopies.[15−18] The set of FTC diagrams for any given noisy-light-based nonlinear optical spectroscopy represents the decomposition of that spectroscopy into its most elementary "physically" meaningful components. The FTC diagrams allow one to greatly organize and simplify rather extensive calculations. In fact, several principles of FTC diagram analysis have been developed which allows one to extract much information from them without the need to perform any calculations.

The mathematics of time domain noisy light spectroscopy (in the perturbative limit) has been presented and discussed in much detail.[1,12,22] The original work[1−3] assumed a δ-function correlation for the noisy field (i.e., a white light limit) and proceeded with perturbatively evolving the density operator in the standard way[54] (with the complication that stochastic averaging over the noise must be done at the intensity level) to obtain a material response. Later models gave Lorentzian[15,22] and Gaussian[22] spectra to the noisy light which added to the computational difficulty but offered further insights. Although mathematics is the most precise language in which to examine noisy light phenomena, a main goal of this paper will be to present more physical considerations, which serve to augment the mathematical foundation already laid, and to give some tangible insight to the equations and underlying physics. These ideas are also helpful in organizing and exposing the potential errors in calculations.

This work begins by establishing some preliminary concepts that will aid us in understanding subsequent ideas. Following this, several physical concepts are set forth in a general way but with particular examples to give concreteness the ideas. The developed physical concepts are then used in the description of the coherent anti-Stokes Raman scattering signal using noisy light (called $I^{(2)}$CARS). $I^{(2)}$CARS is developing into arguably one of the most useful applications of noisy light spectroscopy. Finally, some concluding remarks are made.

II. Preliminary Concepts

Several preliminary ideas must be presented in order to clearly show the basis for the physical description of the noisy light problem and its connection to the mathematical formulation. These include brief discussions of the bichromophoric model, the mathematical representation of noisy light, the Wiener−Khintchine theorem, the motivation for the use of FTC diagrams, and finally a review of filtered incoherent light.

A. Bichromophoric Model. In nonlinear optical spectroscopies, the signal is usually quadrature detected. That is, the signal intensity (the mod-square of the total field) is the experimentally measured quantity. The total field is the (phase-matched) sum of the signal fields launched from each of the individual chromophores in the sample. The mod-square of this sum is dominated by the cross terms, i.e., fields launched from two distinct chromophores. The total intensity is then very well represented by the sum of all pairwise (two chromophore) contributions. This *bichromophoric model* [22,55,56] leads to, for example, the familiar N^2 dependence of the signal intensity in the coherent nonlinear spectroscopies, where N is the number density of chromophores in the sample. For ordinary nonlinear spectroscopies, this point is not of practical relevance. The jth-order polarization (e.g., $j = 3$ for four-wave mixing) alone is sufficient for describing the nonlinear signal. Going to the intensity level is trivial (it is just the mod-square of the calculated polarization). For noisy light spectroscopies, however, stochastic averaging of the noise at the intensity level requires that special attention be given to the signal intensity. The trivial mod-squaring of the nonlinear polarization is now insufficient. The correlations among the various noisy light field interactions on the two (otherwise independent) chromophores must be explicitly treated. These correlations are fundamental to the understanding of noisy light spectroscopies.

Explicit use of the bichromophoric model requires assigning distinct timelines (t and s) to each of the two generic chromophores α_t and β_s, making up a given pairwise cross term. The two timelines allow for the (in general) different histories of evolution for each chromophore; chromophores α_t and β_s are independent (aside from the correlation between the various field interventions on each). As in traditional nonlinear optical spectroscopies using coherent pulses, the density operator is solved perturbatively to jth-order to give the jth-order polarization (or its Fourier transform) which is taken to quadrature. Upon going to quadrature, the dominant intensity is derived from the cross terms between the polarization on one chromophore (having the t timeline) and that on another (having the s timeline) Subsequent stochastic averaging entangles the t and s time variables in a nontrivial way.[15,22]

B. Noisy Light. The physical noisy light field is expressed as

$$\mathbf{E}(\mathbf{r},t) = \epsilon(\mathbf{r},t) + \epsilon^*(r,t) \tag{1}$$

Here, ϵ is the complex analytic signal[57] associated with $\mathbf{E}$, which is implicitly used to determine the subset of relevant field actions of any given phase-matched spectroscopy. For example, a third-order spectroscopy phase matched along $k_s = k_1 + k_2 - k_3$ calls for three real field actions $\mathbf{E}_1\mathbf{E}_2\mathbf{E}_3$ (ignoring time ordering for simplicity). It is convenient here to work with the complex

analytic signals $\epsilon_1\epsilon_2\epsilon_3^*$ to narrow in on the subset of field actions which contribute to the particular phase-matched signal of interest. It is important to remember that the observed signal is finally obtained by taking the real part of the result obtained using the complex analytic fields. This is taken further in noisy light problems. Here, one considers a signal launched from two chromophores (cf., the bichromophore model) acting in conjugate, for example, $\epsilon_1\epsilon_2\epsilon_3^*$ from one and $\epsilon_1^*\epsilon_2^*\epsilon_3$ from the other (with distinct timelines). A careful treatment of the field in this manner has been presented with special emphasis on the Raman-based spectroscopies.[58]

The focus of this paper is exclusively in the time and frequency domains; spatial considerations are not addressed as cross-spectral purity[57] is assumed. For convenience, the tensor notation is suspended and the treatment is reduced to a scalar one. The wavevectors **k** and **k′** are distinct in order to spatially resolve the signal (through phase matching). However, the angle between them is assumed small so that their general direction of propagation can be taken to be along the *z*-axis allowing the field to be expressed as $\mathbf{E}(\mathbf{r},t) \Rightarrow \mathbf{E}(z,t)$. Appropriate orientational averaging of the elements of the dipole moment vector operator projected onto the identically polarized twin beams leaves an effective scalar transition dipole moment μ and a scalar field $E(z,t)$.

The real scalar noisy field is expressed more explicitly as

$$E(z,t) = E_0 p(t) e^{-i\bar{\omega}t+ikz} + E_0 p^*(t) e^{+i\bar{\omega}t-ikz} \tag{2}$$

where p is a complex stochastic function of time assumed to obey circular complex Gaussian statistics[57] and $\bar{\omega}$ is the central carrier frequency of the field. The normalization constant E_0 is such that $\langle p(\tau)p^*(0)\rangle = \gamma^{(1,1)}(\tau)$, where $\gamma^{(1,1)}(\tau)$ is the normalized second-order complex coherence function[57] for a stationary complex random function (the superscript (1,1) denotes the order of the complex random function and of the complex conjugate of that function in the correlator). On femtosecond time scales, the nanosecond pulses used in noisy light experiments are effectively cw; so, for the theory, noisy light is taken to be cw and so E_0 is constant; but for noisy fields that are (nanosecond) pulsed, E_0 is really a slowly varying function of t.

Taking for simplicity the case in which the only active fields are **B** and **B′**, the electric fields associated with each are

$$E_{\mathbf{B}}(z,t) = E_0 p(t) e^{-i\bar{\omega}t+ikz} + E_0 p^*(t) e^{+i\bar{\omega}t-ikz} \tag{3}$$

and

$$E_{\mathbf{B}'}(z,t) = E_0 p(t-\tau) e^{-i\bar{\omega}(t-\tau)+ik'z} + E_0 p^*(t-\tau) e^{+i\bar{\omega}(t-\tau)-ik'z} \tag{4}$$

respectively. With these definitions, $\tau > 0$ means **B′** lags behind **B**. For cases when there are many fields, the noisy fields that are not delayed during an experiment are labeled $\mathbf{B}_i$, the delayed fields are labeled $\mathbf{B}_i'$, and any monochromatic fields are labeled $\mathbf{M}_i$ (The subscripts are dropped if there is only one such field.)

The total real electric field at a point z_0 at time t is

$$E_{\text{tot}}(z_0,t) = E_{\mathbf{B}_1} + ... + E_{\mathbf{B}_l} + E_{\mathbf{B}_1'} + ... + E_{\mathbf{B}_m'} + E_{\mathbf{M}_1} + ... E_{\mathbf{M}_n} \tag{5}$$

where l, m, and n are the number of times **B**, **B′**, and **M** act, respectively. Thus the jth-order spectroscopy requiring $E_{\text{tot}}(t_1)$-$E_{\text{tot}}(t_2)...E_{\text{tot}}(t_j)$ has potentially $[2(l+m+n)]^j$ terms involving the complex analytic function and its conjugate. This total includes all field orderings and all possible combinations of wavevectors and frequencies. Fortunately, phase matching and spectral filtering greatly reduce this number.[58] As a concrete example, consider the third-order photon echo-like noisy light experiment, which is a degenerate four-wave mixing process where **B** acts twice and **B′** acts once. This was the first noisy light experiment to be reported.[1-3] Here, $E_{\text{tot}}(z_0,t) = E_{\mathbf{B}} + E_{\mathbf{B}'}$ now from the above $j = 3$, $l = 1$, $m = 1$, and $n = 0$. Thus, there are $[2(1+1)]^3 = 64$ field products at the complex analytic signal level.

C. Wiener−Khintchine Theorem and Color Locking. The Wiener−Khintchine (WK) theorem is expressed as

$$\gamma^{(1,1)}(\tau) = \langle p(\tau)p^*(0)\rangle = \int_{-\infty}^{\infty} dq\, J(q) e^{-iq\tau} \tag{6}$$

where $J(q)$ is the spectral density of the random function p. The WK theorem states that a two-point (pair) time correlator may be expressed as the Fourier transform of the spectral density of the random process.

An extremely important consequence of stationarity and the WK theorem can be seen by examining a pair correlator in frequency space.[57] Here

$$\begin{aligned}\langle \tilde{p}(q)\tilde{p}^*(q')\rangle &= \left\langle \int_{-\infty}^{\infty} p(t) e^{iqt}\, dt \int_{-\infty}^{\infty} p^*(t') e^{-iq't}\, dt' \right\rangle \\ &= \int_{-\infty}^{\infty} dt' \,\langle p(t)p^*(t')\rangle e^{iq(t-t')} e^{i(q-q')t'} \\ &= \int_{-\infty}^{\infty} \gamma^{(1,1)}(\tau) e^{iq\tau}\, d\tau \int_{-\infty}^{\infty} dt' \, e^{i(q-q')t} \\ &= J(q)\delta(q-q')\end{aligned} \tag{7}$$

where the change of variables $(t, t') \Rightarrow (\tau = t - t', t')$ was used in going to the third line and both the WK theorem and the integral definition of the δ-function were used to obtain the final result. In the context of noisy light spectroscopy, the physical interpretation of eq 7 is that, within the same beam, light of different frequencies (colors) are uncorrelated for stationary noisy light. This is the mathematical expression for *color locking*.

D. Need for FTC Diagrams. The interpretation of the nonlinear optical signal is more complicated for noisy light spectroscopies than it is for coherent short pulse experiments. There are two main reasons for this. First, the length of the pulses is essentially cw on the femtosecond time scale; hence, all fields involved in producing the signal are present at all times. The second is the necessity to stochastically average over the noise at the mod-square (intensity) level (cf., the bichromophoric model). Nonetheless, the first step in interpreting the signal is the same as for short pulse experiments and involves considering the term appropriate to the order of the nonlinear spectroscopy in the perturbative expansion of the density operator.

1. Material Response. Regardless of the light source used to probe the material, it is necessary to begin with all the terms of the density matrix describing the spectroscopy of interest. In general, for a jth-order spectroscopy there are $2^j j!$ terms in the expansion of the density matrix. The 2^j factor arises from the number of distinct Liouville paths,[54] and the $j!$ factor comes from the number of possible field orderings. Several diagrammatic methods have been developed for keeping track of the density matrix terms.[59] The diagrammatic technique employed here is that of Lee and Albrecht.[60] This technique has the advantage that resonances are immediately seen without losing the sense of time evolution. The technique involves drawing a solid horizontal line for real states of the chromophore and dashed lines for virtual states. Solid (dashed) arrows represent

ket (bra) evolution with an upward-pointing arrow representing the action of the positive (negative) Fourier component. These diagrams are called wave mixing energy level (WMEL) diagrams. WMEL diagrams are drawn the same way for both coherent short pulse and noisy light spectroscopies. The only distinction at this point lies in which diagrams are the most important or which may be eliminated due to field orderings. Often the field orderings for coherent short pulse spectroscopies are (assumed) experimentally fixed due to explicit time ordering in the laboratory and an immediate reduction in the number of terms is possible. For noisy light spectroscopies, all field ordering must be considered. The material response is contained in the kernel of the integral equations of motion of the density matrix elements. For any given pair of levels, there is a characteristic (Bohr) frequency and an associated decay parameter describing the "dark" two-state kinetics. The total material response is a sum over all transition dipole weighted pairs of levels. The subject of material response is an area of very active research. Understanding the mechanisms involved in coherence and population decay is of great theoretical and applied interest.

2. Light Response. The point at which the two types of ultrafast spectroscopies diverge is with regards to the behavior of the light. We have seen above that the noisy light develops the *j*th-order density matrix on a chromophore; however, the signal produced by this polarization is itself a stochastic function of time. Since the signal is typically at optical frequencies, it must first be taken to quadrature (to the intensity level) and then averaged over the complex noise. Recall that, upon going to quadrature, the dominant intensity is derived from the cross terms between the polarization on one chromophore and that on another (cf., the bichromophoric model). The stochastic averaging over the noisy light fields is now superimposed and appears as a 2*n*-point time correlator, where *n* is the number of noisy field interventions in the development of the *j*th-order polarization. This correlator may couple the evolutionary histories of the two involved chromophores. This differs from short pulse calculations in which the histories (*t* and *s* timelines) are not coupled and hence integration over only one of them yielding the nonlinear polarization is required. The usual assumptions about the nature of the noise (circular complex Gaussian statistics) and the complex Gaussian moment theorem allow the 2*n*-point time correlator to be broken down into *n*! "factorized" terms each having *n* factors of two point time correlators, which are mathematically much easier to handle. Each of these *n*! intensity level factorized term is represented diagrammatically by an unique FTC diagram.

3. FTC Diagrams. In general, there is a defined correspondence between any given intensity level factorized term composing the noisy light signal and its FTC diagram, i.e., one can draw a diagram for each of the multiplets of two-point (pair) correlators that can arise in nonlinear spectroscopies based on noisy light. A FTC diagram consists of a template of *s* and *t* timelines (the evolutionary histories of the involved chromophores) each with one tick marking the time of each of the *n* noisy field interventions. Superimposed are *segments* (arrows or lines) linking the times contained in each two-point correlator. A τ-dependent pair correlator is represented by an *arrow* segment pointing to the tick mark corresponding to the action of the time-delayed field **B′**. A τ-independent pair correlator is represented by a *line* segment connecting the two time points contained in the pair correlator. The rules for constructing a FTC diagram may be found in Appendix B of ref 15.

Clearly, from the standard definition of a pair correlator (its vanishing at infinite time intervals) and the fact that any FTC diagram represents a product of pair correlators, the contribution to the total signal from all FTC diagrams that contain one or more arrows must vanish as $\tau \rightarrow \infty$ leaving only the background terms (the FTC diagrams having no arrows) in this limit. On the other hand, at $\tau = 0$ all *arrows* turn into *lines* to join the constant background FTC diagrams. When used in conjunction with the WMEL diagrams, this allows for trivial determination of the peak to background contrast ratio of the interferogram for any given spectroscopy. Basically, the characteristics of the final interferogram are a result of two main components: the material response (the WMEL diagrams) and the light response (the FTC diagrams) along with the interplay between the two responses.

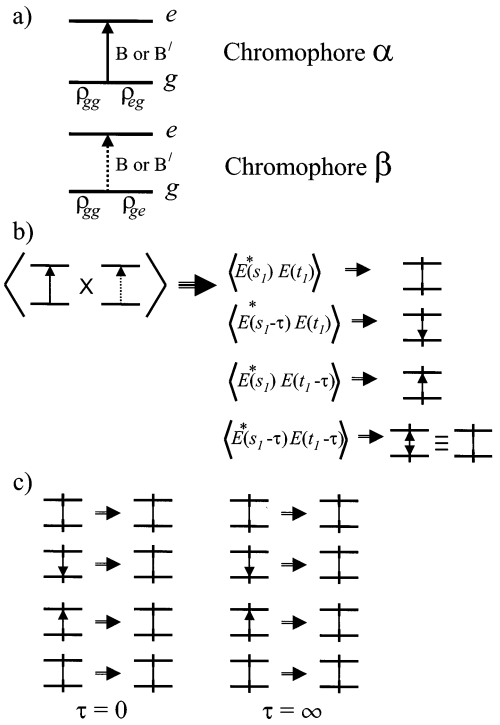

Figure 1. Illustration of how to obtain the FTC diagrams for a noisy light spectroscopy. (a) The WMEL diagram for first-order resonant interaction of light and matter. The solid upward-pointing arrow represents ket-side promotion of the density operator via the positive Fourier component of the field. The dashed upward-pointing arrow represents bra-side promotion of the density operator via the negative Fourier component. The action on chromophore β is conjugate to that of chromophore α. (b) The two amplitude or field level polarization terms represented by the WMEL diagrams of (a) are multiplied and stochastically averaged. Since either **B** or its delayed twin **B′** may act, one obtains four-field pair correlators. Each one of these is represented by a FTC diagram. The first and last terms are τ-independent and thus have FTC diagrams with only line segments. The second and third terms are τ-dependent and therefore have arrow segments in their FTC diagrams. In either case, the times of the correlated field actions t_1 and s_1, for this example, are represented on the FTC diagram as tick marks that are connected by either line or arrow segments. (c) The peak-to-background ratio is obtained readily from the FTC diagrams. At $\tau = 0$ all arrow segments are equivalent to line segments, and at $\tau = \infty$ the terms represented by FTC diagrams having only arrow segments vanish.

As a very simple example of setting up the FTC diagrams for a noisy light spectroscopy, consider the case of first-order resonant light−matter interaction. The first WMEL diagram in Figure 1a shows the action of the positive Fourier component of the field in promoting the ket-side of the density operator from state g to state e (represented in the WMEL diagram by a solid arrow pointing upward). This occurs on chromophore α at time t_1 and the field action can come either from **B** or its delayed twin **B′**. The conjugate process is happening at time s_1

on chromophore β. Here the negative Fourier component promotes the density operator bra-side (represented in the WMEL diagram as an upward dashed arrow). At the intensity level, the polarizations developed on chromophores α and β are multiplied and stochastically averaged as indicated by the left side of Figure 1b. Since each field action may originate from **B** or **B′**, there are four field products that would appear as pair correlators in the calculation of this term (indicated by the middle of Figure 1b). The corresponding FTC diagrams are shown adjacent to each of these terms. Figure 1c shows that at $\tau = 0$ all the arrows in the FTC diagrams become lines and at $\tau = \infty$ all the diagrams that contain arrows vanish. Since the four diagrams at $\tau = 0$ are topologically equivalent to the two FTC diagrams at $\tau = \infty$ the peak-to-background ratio for this example is readily seen to be 2:1. Of course more information than just the peak-to-background ratio can be obtained from the set of FTC diagrams. In section III, several conceptual tools which give insight into the physical mechanisms involved in noisy light spectroscopy will be derived from the FTC diagrams.

E. Filtered Incoherent Light. We now seek to examine the effect of filtering on the coherence function.[61] Upon filtering, the unfiltered stochastic part of the field in frequency space $\tilde{p}(\omega)$ becomes $\vartheta(\omega)\tilde{p}(\omega)$, where $\vartheta(\omega)$ is a deterministic complex amplitude transmission function. The spectrum of the filter is $\vartheta(\omega)\vartheta^*(\omega) \equiv \mathrm{Y}(\omega)$. That is, $\mathrm{Y}(\omega)$ is the (intensity level) output of the filter for a random input. Likewise, $\vartheta(\omega)\tilde{p}(\omega)$ is the (field-level) output for a $\tilde{p}(\omega)$ input field.

At the intensity level, the stochastically averaged filtered light is

$$\begin{aligned}\langle\vartheta(\omega)\tilde{p}(\omega)\vartheta^*(\omega')\tilde{p}^*(\omega')\rangle &= \vartheta(\omega)\vartheta^*(\omega')\langle\tilde{p}(\omega)\tilde{p}^*(\omega')\rangle \\ &= \mathrm{Y}(\omega)J(\omega)\delta(\omega-\omega')\end{aligned} \tag{8}$$

where, in the first step, the transmission functions were pulled out of the brackets because they are deterministic functions and, in the second step, eq 7 was used. The complex second-order coherence function for filtered light is defined as[57,61]

$$\gamma_{\mathrm{Y}}^{(1,1)}(\tau) \equiv \int J_{\mathrm{Y}}(\omega)\mathrm{e}^{-i\omega\tau}\,\mathrm{d}\omega \tag{9}$$

where $J_{\mathrm{Y}}(\omega) \equiv \mathrm{Y}(\omega)J(\omega)$. For situations where $\mathrm{Y}(\omega)$ is much narrower than $J(\omega)$, $J(\omega)$ is relatively flat over the much sharper peaked part of $\mathrm{Y}(\omega)$, so $J(\omega) \approx J(\bar{\omega}_{\mathrm{Y}})_{\mathrm{Y}}(\omega)$, where $\bar{\omega}_{\mathrm{Y}}$ is the center frequency of the filter. Equation 9 then becomes

$$\gamma_{\mathrm{Y}}^{(1,1)}(\tau) = J(\bar{\omega}_{\mathrm{Y}})\int \mathrm{Y}(\omega)\mathrm{e}^{-i\omega\tau}\,\mathrm{d}\omega \tag{10}$$

The spectral density of the light is effectively replaced by the spectral density of the filter in determining the coherence function (compare eqs 6 and 10).

As an example, consider a four-point time correlator in frequency space for filtered light:

$$\begin{aligned}&\langle\vartheta_{\mathrm{a}}(\omega_1)\tilde{p}(\omega_1)\vartheta_{\mathrm{b}}(\omega_2)\tilde{p}(\omega_2)\vartheta_{\mathrm{a}}^*(\omega_1')\tilde{p}^*(\omega_1')\vartheta_{\mathrm{b}}^*(\omega_2')\\ &\tilde{p}^*(\omega_2')\rangle\mathrm{e}^{i(\omega_1-\omega_2')\tau} = \vartheta_{\mathrm{a}}(\omega_1)\vartheta_{\mathrm{b}}(\omega_2)\vartheta_{\mathrm{a}}^*(\omega_1')\vartheta_{\mathrm{b}}^*(\omega_2')\langle\tilde{p}(\omega_1)\tilde{p}(\omega_2)\\ &\tilde{p}^*(\omega_1')\tilde{p}^*(\omega_2')\rangle e^{i(\omega_1-\omega_2')\tau} = \vartheta_{\mathrm{a}}(\omega_1)\vartheta_{\mathrm{b}}(\omega_2)\vartheta_{\mathrm{a}}^*(\omega_1')\\ &\vartheta_{\mathrm{b}}^*(\omega_2')e^{\mathrm{i}(\omega_1-\omega_2')\tau}(\langle\tilde{p}(\omega_1)\tilde{p}^*(\omega_1')\rangle\langle\tilde{p}(\omega_2)\tilde{p}^*(\omega_2')\rangle +\\ &\langle\tilde{p}(\omega_1)\tilde{p}^*(\omega_2')\rangle\langle\tilde{p}(\omega_2)\tilde{p}^*(\omega_1')\rangle)\end{aligned} \tag{11}$$

where the complex Gaussian moment theorem was used in going to the last step. The transmission functions ϑ_{a} and ϑ_{b} are not necessarily the same. This example is representative of what one encounters in the analysis of $\mathrm{I}^{(2)}$CRS. Consider the first term in parentheses and use eq 7

$$\begin{aligned}&\vartheta_{\mathrm{a}}(\omega_1)\vartheta_{\mathrm{b}}(\omega_2)\vartheta_{\mathrm{a}}^*(\omega_1')\vartheta_{\mathrm{b}}^*(\omega_2')\langle\tilde{p}(\omega_1)\tilde{p}^*(\omega_1')\rangle\langle\tilde{p}(\omega_2)\\ &\tilde{p}^*(\omega_2')\rangle\mathrm{e}^{i(\omega_1-\omega_2')\tau} = \vartheta_{\mathrm{a}}(\omega_1)\vartheta_{\mathrm{b}}(\omega_2)\vartheta_{\mathrm{a}}^*(\omega_1')\vartheta_{\mathrm{b}}^*(\omega_2')J(\omega_1)\delta(\omega_1 -\\ &\omega_1')J(\omega_2)\delta(\omega_2-\omega_2')e^{i(\omega_1-\omega_2')\tau}\end{aligned} \tag{12}$$

Transforming to the time domain, this becomes

$$\begin{aligned}&\int \mathrm{d}\omega_1 \int \mathrm{d}\omega_2 \int \mathrm{d}\omega_1' \int \mathrm{d}\omega_2'\, \vartheta_{\mathrm{a}}(\omega_1)\vartheta_{\mathrm{b}}(\omega_2)\vartheta_{\mathrm{a}}^*(\omega_1')\vartheta_{\mathrm{b}}^*(\omega_2')\\ &J(\omega_1)\delta(\omega_1-\omega_1')J(\omega_2)\delta(\omega_2 -\\ &\omega_2')\mathrm{e}^{i(\omega_1-\omega_2')\tau}\mathrm{e}^{i(-\omega_1-\omega_2+\omega_1'+\omega_2')t} =\\ &\bar{J}\int \mathrm{d}\omega_1 \int \mathrm{d}\omega_2\, \vartheta_{\mathrm{a}}(\omega_1)\vartheta_{\mathrm{b}}(\omega_2)\vartheta_{\mathrm{a}}^*(\omega_1)\vartheta_{\mathrm{b}}^*(\omega_2)\mathrm{e}^{i(\omega_1-\omega_2)\tau} =\\ &\bar{J}\int \mathrm{d}\omega_1\, \mathrm{Y}_{\mathrm{a}}(\omega_1)\mathrm{e}^{i\omega_1\tau}\int \mathrm{d}\omega_2\, \mathrm{Y}_{\mathrm{b}}(\omega_2)\mathrm{e}^{-i\omega_2\tau}\end{aligned} \tag{13}$$

where the trivial integrations have been performed and the integrals separated; $\bar{J}$ is a constant (cf., eq 10). This is a product of a Fourier transform and a conjugate Fourier transform. To progress further with this example, for simplicity, δ-function filters at different frequencies will be used [$\mathrm{Y}_{\mathrm{a}}(\omega_1) = \delta(\omega_1 - \bar{\omega}_{\mathrm{a}})$; $\mathrm{Y}_{\mathrm{b}}(\omega_1) = \delta(\omega_1 - \bar{\omega}_{\mathrm{b}})$]. Equation 13 then becomes

$$\begin{aligned}&\int \mathrm{d}\omega_1\, \delta(\omega_1-\bar{\omega}_{\mathrm{a}})\mathrm{e}^{i\omega_1\tau}\int \mathrm{d}\omega_2\, \delta(\omega_1-\bar{\omega}_{\mathrm{b}})\mathrm{e}^{-i\omega_2\tau} =\\ &\mathrm{e}^{i\bar{\omega}_{\mathrm{a}}\tau}\mathrm{e}^{-i\bar{\omega}_{\mathrm{b}}\tau}\end{aligned} \tag{14}$$

Upon taking the real part, this becomes $\cos \Delta_{\mathrm{ba}}\tau$, where $\Delta_{\mathrm{ba}} \equiv \bar{\omega}_{\mathrm{a}} - \bar{\omega}_{\mathrm{b}}$.

The above example shows the coherence function of filtered light that originally was broad, but of otherwise arbitrary form, can show difference beats with a period equal to the separations of the nominal centers of the filters. This forms the basis of the spectral filter analogy to be applied to coherent Raman scattering with noisy light later in this work.

III. Physical Concepts

Now that the preliminary concepts have been presented, we shall attempt to develop a deeper intuitive understanding of the physics describing the interaction of noisy light and matter and the role of classical field correlations in noisy light spectroscopy. Explicit examples will augment the discussion of general concepts.

A. Conceptual Tools Provided by the FTC Diagrams. The noisy nature of the light which is vital to all noisy light spectroscopies blurs the physical picture of the underlying mechanisms that make up this interesting area of physics. Not only does a new layer of analytic challenge appear but perhaps more interesting is the challenge to clarify the physical aspects of the treatment. Doing this will result in a more intuitive picture of noisy light spectroscopy. As stated above, it is believed that (for stationarity and circular complex Gaussian statistics) the FTC diagrams represent elementary physical components of noisy light spectroscopies in general. That is, the FTC diagrams represent terms in the analytic expression for the total signal that have elementary physical interpretation. Any further breakdown of the analytic expression would seem to lose such physical meaning. One now seeks a more revealing understanding of the FTC diagrams by developing several conceptual tools.

1. Preferred Region. The first of these tools involves the nature of the light. The electric field of the noisy light forms a

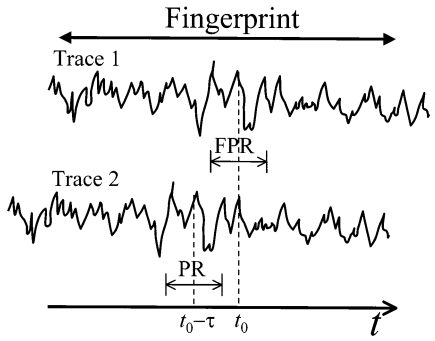

Figure 2. Illustration of the preferred region. The electric field envelope of two identical but relatively delayed light beams are shown. A given noisy light trace, 1, has a distinctive fingerprint; any given section of duration τ_c is referred to as a fingerprint region (FPR in figure). The preferred region (PR in figure) is a special fingerprint region on noisy light trace 2 associated with a given point on trace 1, i.e., the center time point of the preferred region on trace 2 exactly matches the given point on trace 1. Were trace 1 to perturb the system at time t_0, then the "preferred" time for trace 2 to act would be the approximately τ_c long time interval around time $t_0 - \tau$.

unique random pattern as a function of time. One might call this its "fingerprint." Now, for any given nanosecond light pulse, **B**′ will have exactly the same fingerprint as that of **B**, only it is shifted in time by τ. When this time shift is within the coherence time of the light (as long as $|\tau| < \tau_c$), the twin beams **B** and **B**′ "recognize" that they originate from the same source and their overlap results in high interferometric contrast (i.e., strong constructive and also strong destructive interference). So an approximately τ_c long section of the noisy light trace is the shortest interval which gives a distinctive fingerprint region. Equivalently, if one were to examine the fingerprint region of the beam **B** around some moment in time t_0 (measured from a laboratory reference), one would find the identical fingerprint region in beam **B**′ only centered in time at $t_0 - \tau$. Were beam **B** to perturb the system at t_0, then the "preferred" time giving the concerted action of twin **B**′ would be the region around $t_0 - \tau$ for optimal interferometric contrast. This region is designated the *preferred region*. Figure 2 illustrates the important aspects of the concept.

The most basic experimental manifestation of the preferred region is illustrated with a simple interferometric autocorrelation. Here the twin noisy beams **B** and **B**′ are made collinear as they exit the Michelson interferometer and the intensity of this collinear beam is recorded versus the relative delay τ between **B** and **B**′. The resultant interferogram is shown in Figure 3, which clearly illustrates the high interferometric contrast seen when $\tau < \tau_c$. At a given instant t_0, the τ-dependent part of the intensity results from the field **B** being taken to quadrature with field **B**′. At t_0, **B**′ offers a net constructive overlap of the noisy envelope of the twin fingerprint regions associated with the identical fingerprint region centered about t_0 only when $|t_0 - \tau| < \tau_c$. The τ-independent background results from the quadrature contributions from both **B** itself ($|B|^2$) and **B**′ itself ($|B'|^2$), hence, trivially achieving perfect overlap of the noise. It should be noted that for certain noisy light experiments the τ-independent background will be strongly suppressed.[15]

2. Time Symmetry. The second conceptual tool involves the time symmetry of the elementary components (here referring to the light and the material response) of the interferogram. The time symmetry of the noisy field is rooted in the nature of the preferred region. The preferred region has *two-sided time symmetry*. In other words, if **B** happened to have acted upon a chromophore at laboratory time t_0, then the "preferred" time

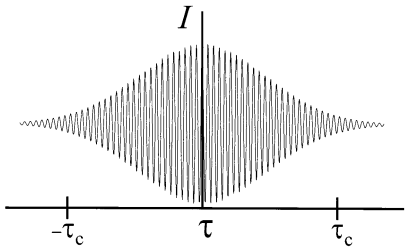

Figure 3. Simulation of a simple interferogram under white detection. Here the two noisy light fields **B** and **B**′ are simply superimposed on the detector and the intensity is plotted as a function of the interferometric delay time τ. One sees high interferometric contrast when τ is small ($|\tau| < \tau_c$). This interferometric contrast diminishes as the relative delay between **B** and **B**′ becomes large ($|\tau| > \tau_c$). For typical noisy light sources τ_c is on the order of 100 fs or so. This provides the ultrafast time resolution of noisy light methods. For this work a precise mathematical definition of τ_c is not important. Only the physical idea of τ_c representing the relative delay time after which two identical noisy beams are effectively uncorrelated is important. The marks on the τ axis at $\pm\tau_c$ simply emphasize this physical notion of τ_c.

for **B**′ to join **B** in a concerted action is centered around laboratory time $t_0 - \tau$ such that action at $(t_0 - \tau) - \epsilon$ (where ϵ is a time $<\tau_c$) is equally "preferred" to action at $(t_0 - \tau) + \epsilon$. The two-sided time symmetry of the noisy light is seen experimentally in the autocorrelation of Figure 3. By contrast, in this same sense the material response function of the chromophore has *one-sided time symmetry*. As an example, in the Bloch two-level system one encounters a simple coherence response and a population response. First, a field action at time t_1 on the chromophore in the ground state (the first field intervention) may cause an electronic polarization which will subsequently decay with a dephasing rate constant γ_{mg}. Next, a second field intervention can build on this polarization to create an excited-state population, which then will decay with rate constant γ_{mm}. Both events have one-sided time symmetry. If the first field acts on the chromophore at time t_1, then at $t_1 - \epsilon$ there is no polarization while at time $t_1 + \epsilon$ there is a polarization. Likewise, if the second field acts at t_2 then at $t_2 - \epsilon$, there is only a polarization but at $t_2 + \epsilon$ there is a population.

The autocorrelation shown in Figure 3 is identical to the one that would be seen by a short pulse having the same spectrum (albeit phase-locked). We see that in some sense the preferred region is like a short pulse. Indeed, in practice, noisy light has been described as a random train of short pulses. One must use this description with great caution however, since short pulses imply at least some sort of phase locking. Phase locking further implies that color locking does not hold. This will lead one to results that are not consistent with experiment. Color locking is indeed a fundamental attribute of noisy light.

3. Accumulation. Across the ensemble of chromophores the noisy fields (and narrowband fields if any) may act on a given ensemble member at any time during the pulse duration. For those sequences of field actions that contribute to the signal of interest, this ability for the fields to act at any time on a given chromophore must be summed over the ensemble of chromophores participating in producing the signal of interest. From a topological point of view this is represented on an FTC diagram as the freedom of a tick mark to "slide along a timeline". Since **B** and **B**′ are "always" present, any time intervention (tick mark on the FTC diagram) or any pair of interventions is free to slide along the timeline provided the specific time ordering associated with a given FTC diagram is maintained. That is, during the sliding along the timeline, tick marks cannot cross one another. To "slide along the timeline" indicates the potential for field action to take place at any time

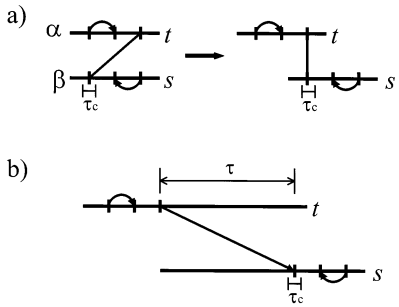

Figure 4. Illustration of synchronization. Interchromophoric pair correlators synchronize the otherwise independent time histories of chromophores α_t and β_s. The strength or precision of the synchronization is τ_c. The top (bottom) horizontal line of the FTC diagram represents the timeline for α_t (β_s). The tick marks are the times when the noisy light interacts with the material. (a) The right-hand diagram is representative of what a typical FTC diagram for a nonlinear process would look like. This particular FTC diagram represents a term in which there is τ-dependent correlation between time t_1 and t_2 and between s_2 and s_3. Additionally, there is τ-independent correlation between the timelines (t_3 and s_1). The τ-independent correlator (line) synchronizes the timelines such that the two time points involved in the correlator are coincident. (b) This FTC diagram is similar to that of (a) but now the interchromophoric correlation is also τ-dependent. This τ-dependent correlator (arrow) synchronizes the timelines such that the two points involved in the pair correlator are separated by exactly τ.

over which the tick mark is permitted to slide. However, an individual tick mark is locked to a partner tick mark by the segment (arrow or line) representing a pair correlator. The two tick marks, thus linked, correspond to a correlated event pair that must slide along the time line together. This ability to "slide along the timeline" will be referred to as *accumulation*. Physically, accumulation represents the summation over the ensemble of chromophores in which the correlated noisy field interventions have the ability to act at anytime relative to the other (nonpair correlated) action(s) that produce the final nonlinear signal. Mathematically, it represents integration over the time intervals between the light−matter interactions.

4. Synchronization. The fourth conceptual tool is concerned with the event coupling between the two timelines (*t* and *s*). This coupling involves interchromophoric pair correlators. It has been noted how all of the τ-independent correlators are depicted by lines. These correspond to the correlated action of **B** with itself and **B′** with itself. This implies tight synchronization between the two chromophores of the events linked by a given correlator line. The "precision" or "strength" of this synchronization is inversely proportional to τ_c (the interferometric width of the preferred region). That is, small τ_c forces strong or precise synchronization with the limit of $\tau_c \rightarrow 0$ forcing exact synchronization. When τ_c is much smaller than the dynamics of the media, it is convenient to use the $\tau_c \rightarrow 0$ limit. Synchronization is shown in Figure 4a for τ-independent interchromophore correlation. The τ-dependent correlators are represented by arrow segments. These correlate the action of field **B** with **B′**. Interchromophore synchronization has the same meaning for arrowed segments; however, a very important subtlety must be exposed. The synchronization of the *s* and *t* timelines are still to within a "precision" of roughly τ_c, but now there is a translation in time by the delay line setting τ. For example, if **B′** lags behind **B** for positive τ and an arrow couples t_1 (B acting) and s_1 (B′ acting), then on an absolute laboratory timeline $s_1 \stackrel{p}{=} t_1 + \tau \pm \tau_c$, where $\stackrel{p}{=}$ means "prefers to equal." The concept of prefers to equal arrises from considering the behavior of the ensemble. This is discussed in detail in a later section. For a given action of **B** at time t_1, the preferred time

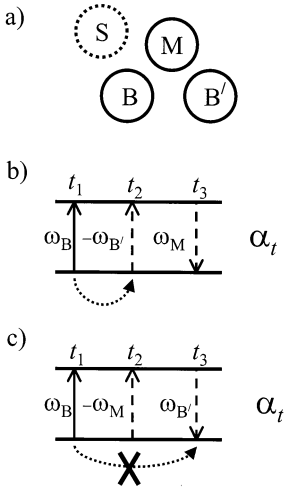

Figure 5. An example of a degenerate four wave mixing experiment using two noisy fields **B** and **B′** and a narrowband field (**M**). See text for more details. (a) A projection of the input and signal light beams on a plane perpendicular to the direction of propagation. The signal emerges at $\mathbf{k}_s = \mathbf{k}_B - \mathbf{k}_{B'} + \mathbf{k}_M$. (b) One of the 48 WMEL diagrams for this process. The WMEL diagram represents one term in the perturbative expansion of the density operator for the field interacting with a generic chromophore α. The vertical arrows represent ket-side and bra-side transitions. The direct correlation between the noisy field actions is subject to color locking. This results in complete cancellation of the noise, and the resulting signal spectrum has narrow bandwidth. (c) A WMEL diagram for an alternative four-wave mixing process, $\mathbf{k}_s = \mathbf{k}_B + \mathbf{k}_{B'} - \mathbf{k}_M$, in which there is no direct correlation between the noisy field actions on a given chromophore. Hence, color locking is not required and the resulting signal has a broad bandwidth.

region for the action of **B′** on the *s*-line is $s_1 \stackrel{p}{=} t_1 + \tau \pm \tau_c$. This subtlety allows for indirect correlation (to be discussed shortly) and has very significant effects on coherent Raman scattering experiments. It is illustrated in Figure 4b.

5. Color Locking. The final conceptual tool, color locking, follows from stationarity and the WK theorem (see eq 7). It implies that, regardless of the spectral density of the sources, only identical frequencies (colors) may correlate to one another in a pairwise fashion. The consequence of color locking to FTC diagram analysis is that, whichever frequency component happens to act, from one field of a correlated pair (represented by one end of a line or arrow) the other field of the correlated pair (represented by the other end of the line or arrow) must act with the same frequency component. This allows one to maintain the use of correlator terminology for a single color and refer to a $x-x$ color-locked pair correlator, where x is a single frequency component of the noisy light.

Color locking manifests itself in many ways and is fundamental to understanding noisy light signals. One such example (shown in Figure 5) is that of a degenerate four-wave-mixing experiment in which **B** and **B′** act out of phase and the third field is a narrowband field ($\mathbf{k}_s = \mathbf{k}_B - \mathbf{k}_{B'} + \mathbf{k}_M$). This is sometimes referred to as forced light scattering.[6] From simple frequency mixing algebra, one might naively expect the spectrum of the signal to be centered at $\bar{\omega}_s = \bar{\omega} - \bar{\omega} + \omega_M$ and to carry the width of the noisy fields. Color locking forbids this however since the out-of-phase actions of **B** and **B′** are correlated and hence on any given chromophore only the precise frequency x from both **B** and **B′** may act. Inspection of a representative WMEL diagram for this process (shown in Figure 5) clearly reveals that the out-of-phase action of the single frequency cancels. This holds for all frequencies x, so the noise, in fact, cancels, and one is left with simply the bandwidth of the narrowband field. By contrast, the relatively much weaker

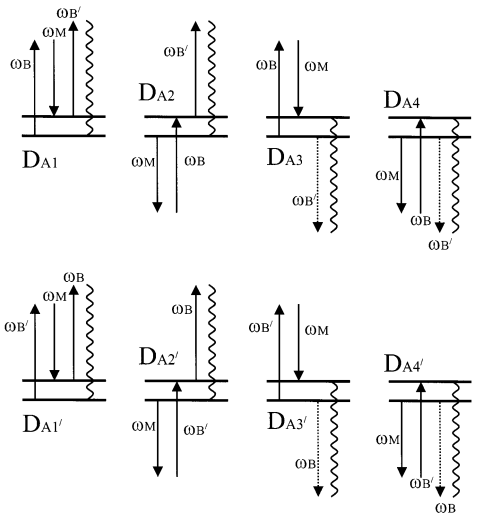

Figure 6. The 8 of the 48 WMEL diagrams for $I^{(2)}$ CARS that have a Raman resonance after the second field intervention. Diagrams D_{Ai} and $D_{Ai'}$ are identical except for the reversal of the interaction ordering of **B** and **B′**.

in-phase degenerate four-wave mixing signal is shown in Figure 5c. Here the in-phase noisy field actions are not pair correlated and hence not color-locked. This results in no noise cancelation and thus in a broad signal spectrum seen experimentally. Later, we shall see that color locking has particularly significant but more subtle effects for (in-phase) interchromophoric correlations.

B. Spectral Filter Analogy. It is interesting and insightful to view the material as a nonlinear filter of the noisy light. (More correctly, the material is a nonlinear "selective frequency enhancer.") This *spectral filter analogy* is pursued in the context of electronically nonresonant $I^{(2)}$CARS experiment but does apply generally. $I^{(2)}$CARS spectroscopy involves a single intervention of a narrow band beam along with interventions by **B** and **B′** (fields that act mutually in phase but out of phase with respect to the narrow band field **M**). Furthermore, the signal is dominated by those terms which enjoy a Raman resonance. The corresponding Raman resonant WMEL diagrams for the $I^{(2)}$CARS process are shown in Figure 6. A common characteristic of these diagrams is that the first two steps (field interventions) always involve one noisy field action and the narrow band field action, which are effectively simultaneous for the electronically nonresonant case. It is now convenient to develop several definitions. We consider the first two steps, after which there is a Raman resonance, to make up the first *stage* of the $I^{(2)}$CARS process. These first two steps will be referred to collectively as *stage1*. The last two steps, the third field intervention and the fourth wave step, will be collectively called *stage2* (of the $I^{(2)}$CARS process). One particular WMEL diagram is redrawn in Figure 7. The Raman resonance after *stage1* is seen to enhance the effectiveness of a small region of the noisy spectrum (centered about $x_0 = \omega_{\mathbf{M}} + \omega_R$) in developing the eventual fourth wave. One particular Raman resonant frequency component x that is selectively enhanced by the Raman resonance is labeled in Figure 7. The bandwidth in which x is contained is on the order of $\gamma_{mg} + \Gamma_m$, which is the sum of the material line width γ_{mg} and the width of the narrow band spectrum Γ_m. Effectively, the choice of x has been "filtered" and takes on a much more restrictive bandwidth; on the order of $\gamma_{mg} + \Gamma_m$, rather than the width of the noisy light spectrum which is parametrized by Γ ($\Gamma \gg \gamma_{mg}$). This effective "filter" (due to the Raman resonance) will be called the *stage1 filter*, since it involves the cooperation of the first two field

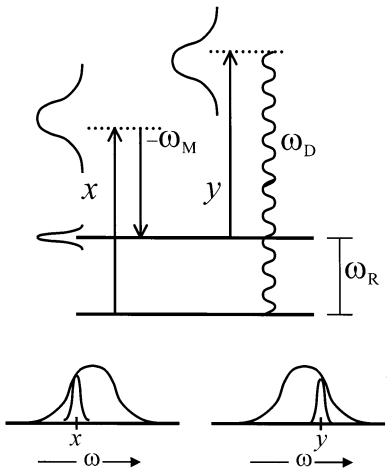

Figure 7. One of the WMEL diagrams for $I^{(2)}$CARS. Only a small subset of frequencies in the noisy light spectrum can couple with $\omega_{\mathbf{M}}$ such that a Raman resonance is achieved after the second field action. This is indicated by the narrow spectrum shown superimposed on the broad spectrum shown below the WMEL diagram. This limitation on the frequencies is called the *stage1* filter. In the final step, although any frequency within the bandwidth of the noisy light can act, only a small subset will produce a signal that will reach the (monochromatic) detector. This again effectively filters the broad spectrum down to a smaller subset. This is called the *stage2* filter. Difference beating between these filtered subsets of frequencies is observed in the interferograms for $I^{(2)}$CARS.

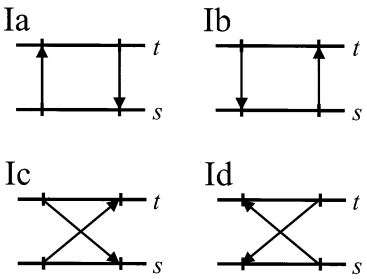

Figure 8. The four τ-dependent FTC diagrams for $I^{(2)}$CARS. Diagrams Ia and Ib are called uncrossed diagrams and Ic and Id are called crossed diagrams. Tick marks are drawn only for noisy light interactions; thus, this third-order process has only two tick marks exposed on the FTC diagram because the narrowband interaction is not shown.

interventions that make up *stage1* of the $I^{(2)}$CARS process. Now, turning to the third step (field intervention), any frequency (labeled y in Figure 7) within the broadband spectrum J may act. Thus, the field launched by the induced third-order polarization [the fourth wave step (wavy line in the WMEL diagrams)] is just as broad as the input noisy fields. When all frequencies of the signal are simultaneously detected (white detection), the interferogram exhibits a rapid monotonic decay with rate Γ. However, if instead, the fourth wave is detected in narrow band mode, the narrow Γ_{slit} bandwidth detected frequencies together with the Raman resonance (*stage2*) act as a second narrow band-pass filter (center $y_0 = \bar{\omega}_D - \omega_R$, width $\gamma_{mg} + \Gamma_{slit}$) which greatly limits the frequencies that y may span and still enjoy Raman resonance. This second filter, due to the cooperation of the third field intervention and the narrowband detection, will be called the *stage2 filter*. At this point there is an analogy with the example presented earlier, where the *stage1* and *stage2 filters* play the role of the transmission functions (at the amplitude level). The WMEL diagram in Figure 7 taken to quadrature is represented by one of the "uncrossed" FTC diagrams in Figure 8 (diagrams Ia and Ib). We see that just like the filtered light example, we have a Fourier transform of

the intensity level spectrum of the *stage1 filter* and the conjugate Fourier transform of the intensity level spectrum of the *stage2 filter*.

For example, when all the intensity level spectra (noisy light, *stage1 filter*, and *stage2 filter*) are Lorentzian, the resulting interferogram is of the form Typically, $\Gamma_{\text{slit}}, \Gamma_m \ll \gamma_{mg}$ and this

$$I \propto \underbrace{e^{-(\gamma_{mg}+\Gamma_m)|\tau|}}_{\textit{stage1 filter}} \underbrace{e^{-(\gamma_{mg}+\Gamma_{\text{slit}})|\tau|}}_{\textit{stage2 filter}} \underbrace{\cos(x_0 - y_0)\tau}_{\text{difference beating}} . \quad (15)$$

becomes

$$I \propto e^{-2\gamma_{mg}|\tau|}\cos(x_0 - y_0)\tau \quad (16)$$

The difference frequency $(x_0 - y_0)$ is exactly $(\bar{\omega}_D - \omega_{\mathbf{M}} - 2\omega_R)$. This is the familiar radiation difference oscillation (RDO) common to the narrow-band detected $I^{(2)}$CARS.[20,22,23,27−29] The oscillations are now viewed as difference beating between two filter functions. It should be noted that earlier work (pre ca. 1997) used RDO to stand for Rabi detuning oscillation. The Rabi detuning oscillations and the radiation difference oscillations are exactly synonymous. The change, which was limited by the motivation to preserve the "RDO" initials, was made for two reasons. For one, radiation difference oscillations captures the spirit of the spectral filter analogy and the fact that the difference in *stage1* and *stage2* "filtered" light was the source of the interference beats: the RDOs. Secondly and more importantly, it was pointed out during the review process that Rabi detuning has such a "textbook" definition in the development of the Rabi frequency in elementary quantum mechanics. Although the RDOs are related to the Rabi frequency problem in a general sense, use of the phrase Rabi detuning oscillation might cause unnecessary confusion.

The spectral filter analogy for the "crossed" FTC diagrams (Ic and Id) in the $I^{(2)}$CARS set (Figure 8) is not quite as transparent as for the uncrossed diagram just discussed. For the crossed FTC diagrams, a given color x selected by the *stage1 filter* on chromophore α_t is forced to also appear at *stage2* on chromophore β_s because of the crossed topology of the FTC diagrams and color locking. That is, a pair correlator (arrow segment) for the crossed FTC diagrams connects times t_1 (on α_t) and s_2 (on β_s) and this pair correlator is color-locked as a consequence of stationary field statistics. Similarly, color y selected by the *stage2 filter* on α_t is forced to appear at *stage1* on β_s. Such entanglement complicates the analogy. Shortly however, the physical rationalization of both the crossed and uncrossed FTC diagrams that make up the $I^{(2)}$CARS signal will be taken to a higher level of sophistication by elaborating on the requirement of color locking.

This filter analogy may be applied to electronically resonant spectroscopies as well. However, the electronic material bandwidth transmission function is now often as wide as the noisy light spectrum. Nonetheless, as the noisy beams are detuned from the center Bohr frequency, some of the broadband spectrum no longer overlaps the transmission function, hence, limiting the effective bandwidth and slowing the decay rate of the interferogram. This is one reason the apparent T_2 times measured at different excitation frequencies within an electronic absorption band of the sample are often different: they increase when the broadband light spectrum overlaps with less of the absorption spectrum. It is important to note that these arguments are appropriate only when the states comprising the manifold of the electronically resonant energy band can be treated more or less independently. If there is a strong quantum mechanical coupling between states within the manifold, then this coupling can act to "unlock" the colors and hence moots arguments based on color locking. This is evident in noisy-light-based forced-light scattering where T_2 measurements deviate from what would be expected from simple color locking.[6,62]

C. Wave Packets and Indirect Correlation. We have seen the importance of color locking throughout this paper; however, it brings up an interesting apparent paradox. Since a given frequency component is required to pair correlate only with itself (the identical frequency component), it is completely uncorrelated with any other frequency component in its (or any other) spectrum. It is neither affected by nor affects other colors; it is not phase-correlated (phase-locked) with the other colors. Such color locking necessarily implies an infinite correlation time. Yet most of the interferograms encountered in noisy light do not show infinite correlation. Furthermore the idea of the preferred region depends on this finite correlation time. At first glance, there appears to be a paradox. This is resolved by examining the problem more carefully. We seek to explain why many interferograms decay with increasing $|\tau|$ to a constant background.

First of all, infinite correlation times are in fact observed in the ideally monochromatic detection limits for zeroth-order interferograms; that is, when there is no sample and **B** and **B′** are simply superimposed on the monochromatic detector. In this case, only one pair correlator (one arrow) makes up the FTC diagram. When the monochromatic detector is set at a frequency, $\omega = x$, then the only contribution to the detected signal comes from the $x-x$ color-locked pair correlator (all other frequencies are blocked), and the infinite correlation between x and itself is realized. However, when the monochromaticity of the detector is relaxed, and in particular taken to the limit of white detection, then the signal is a superposition of the continuous distribution over all available colors of the color-locked pair correlators, each having infinite correlation time. Though any given color is infinitely self-correlated, the resultant signal field is a wave packet in τ-space that decays with a rate constant Γ that is proportional to its spectral width. In other words, interferometry with monochromatic detection selects a single Fourier component from the noisy light spectrum which has an infinitely extended sinusoidal correlation function. Opening up the detector to a broader range of frequencies simply superimposes more Fourier components and, hence, more infinitely extended cosine correlation functions, each with a slightly different frequency. This superposition forms a wave packet in τ-space to produce an interferogram that decays to a constant background. White detection always selects for τ-space wave packet behavior regardless of the spectroscopy of interest and leads to finite correlation times.

The more interesting case is when the nonlinear behavior of the material produces decaying interferograms even at the monochromatic detection limit, where (by definition) no τ-space wave packets can be formed. This yields the important conclusion that the material mediates, through nonlinear interaction, the connection between field interventions even when the intervening colors are not the same (and are fully uncorrelated). That is, the material allows for a connection between two field intervention times (at *stage1* and *stage2* in the $I^{(2)}$CARS example) even when those two times are not linked by an arrow (or line) segment in the FTC diagram (i.e., for the $I^{(2)}$CARS example, there is no pair correlator linking the colors selected by the *stage1* and *stage2* filters on a given chromophore.) This concept is most easily seen for uncrossed FTC diagrams of the type shown in Figure 8 (this type appears for $I^{(2)}$CARS among

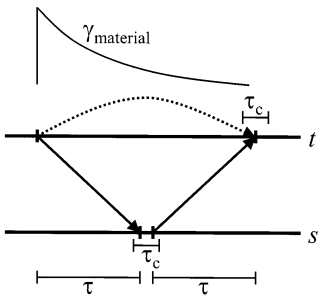

Figure 9. Illustration of indirect correlation. Direct correlation between the first tick marks on each timeline cause the first tick mark on the *s*-timeline to be τ ahead of that on the *t*-timeline. Consequently the second tick mark on the *s*-timeline must be positioned at least τ ahead of the first tick mark on the *t*-timeline. Since the second tick marks on each timeline are correlated, the one on the *t*-timeline must be τ ahead of the one on the *s*-timeline. This results in the topological constraint that the first and second tick marks on the *t*-timeline must be at least 2τ apart. Thus the two tick marks are indirectly correlated because of their direct correlation with events on the *s*-timeline.

others). Here color *x* (from **B**) acts at t_1 (during *stage1*) on chromophore α_t and is correlated to its conjugate action (from τ shifted B′) at s_1 (during *stage1*) on chromophore β_s. One of the uncrossed diagrams is redrawn in Figure 9 for nonzero τ. As τ moves from zero, the arrow (representing the pair-correlated actions of fields **B** and **B′**) prefers to act (with field **B′**) on β_s at a time s_1, such that $(t_1 + \tau - \tau_c) < s_1 < (t_1 + \tau + \tau_c)$. The other color *y* (selected by the *stage2 filter*) acts at s_2 on β_s. It prefers to act on α_t at time t_2, such that $(s_2 + \tau - \tau_c) < t_2 < (s_2 + \tau + \tau_c)$. This effectively forces t_1 and t_2 apart (see Figure 9) (*stage1* and *stage2* are forced apart). We know analytically that the uncrossed type of FTC diagram gives rise to terms which decay in $|\tau|$ with rate constant $2\gamma_{mg}$;[20,22,23,27−29] yet, there is no (solid) arrow segment connecting the two time interventions on the same chromophore, namely, between t_1 and t_2 or s_1 and s_2, which could obviously probe γ_{mg}. This apparent problem is resolved with the help of Figure 9. Here, increasing τ forces the two interventions at time t_1 and t_2 to be separated by at least 2τ; as a result, the contribution of this FTC diagram to the total interferogram decreases (with decay rate constant $2\gamma_{mg}$) as τ is increased even though τ-dependent pair correlators never appear between *stage1* and *stage2* on any given chromophore. (The factor of 2 accounts for the 2-fold gain in the t_1, t_2 separation for increasing τ as per Figure 9.) The same argument holds when making τ more negative, except now it is s_1 and s_2 that are forced apart. So, in this way τ indirectly probes the material dephasing rate γ_{mg} (denoted by the dotted arrow in Figure 9). Although *x* and *y* are not locked to each other through a pair correlator, they are indirectly connected through the event orderings on the chromophores. Hence, this indirect connection introduces a finite correlation to the interferograms even for monochromatic detection. This indirect connection between time points (t_1 and t_2 in our example, Figure 9) will be referred to as *indirect correlation*. Whenever the material is involved in a nonlinear process (multiple field interventions), such that the event orderings force an indirect correlation between different two time points, which do not otherwise form a correlated event pair and may even involve different colors, the resultant interferogram will decay even when the signal is detected in narrowband mode. This decay is probed through such indirect correlation. The phenomenon of indirect correlation is discussed in a more general context and for a variety of FTC diagram topologies elsewhere.[63]

D. Ensemble versus Single Chromophore Thinking and the Preferred Region. Often in nonlinear optics, one does not need to be careful to distinguish between ensemble thinking and single (or few) chromophore thinking. Typically, thinking about a generic chromophore is sufficient for understanding the physics of the process. However, the topic of the preferred region does require a little more care. Above, we have concluded that a color-locked pair at a single frequency is infinitely correlated, and yet we need to refer to a preferred region in which an action of **B** prefers to correlate with an action of **B′**. The preferred region must be viewed in an ensemble sense. Note that in what follows we are not considering the spatial distribution of the chromophores in the ensemble. Spatial considerations do add an extra level of complexity to the problem,[22,55,56] but these effect do not seem to have a dramatic impact on experimental results. Theoretical descriptions of noisy light experiments almost never include the spatial aspect of the interaction volume. Rather than thinking of a single chromophore α_t, one must consider an ensemble of α_t chromophores at some time t_0. Although only one color of, for example, field **B** acts on a given chromophore, all colors from **B** with spectrum $J(\omega)$ are present and act on members of the ensemble of α_t chromophores. Now, it is only when the correlated action of, for example, **B′** on chromophore β_s is summed over the ensemble of β_s chromophores that the preferred region has meaning. It is an "ensemble wave packet" (now in real time rather than in interferometric time) formed by the superposition of the (infinitely extended sinusoidal functions) correlated actions over the β_s chromophores. In other words, at any given time there is a distribution of α_t chromophores which have experienced a field intervention. The number of chromophores acted upon by a given frequency ω is weighted by $J(\omega)$ (the spectrum of the light). Although any given frequency ω from **B** acting on α_t is infinitely correlated with the same frequency ω from **B′** acting on β_s, the combined sum over the weighted distribution of frequencies across the ensemble forms a wave packet. The preferred region is now defined as the unique interval where this maximum interference (wave packet) takes place. This real time ensemble wave packet is precisely analogous to the τ-space wave packet previously discussed, except now it occurs in a space that one is not measuring (i.e., in real time across the ensemble). With this said, it is almost invariably more convenient in practice to think of the preferred region not as this ensemble wave packet but as described previously.

IV. $I^{(2)}$ Cars: An Application of Physical Ideas

Picking up from the spectral filter analogy, this section characterizes the $I^{(2)}$CARS interferogram and spectrum for a pure system (only one chemical species with only one Raman resonance) using only the previously developed physical insights afforded by the FTC diagrams and the WMEL diagrams. The physical description of the $I^{(2)}$CARS signal to follow is inherently less precise than the mathematical one already presented;[20,22,23,27−29] however, it complements the mathematics in that one can now step away from the rigorous constraints of the equations and build a physical model that captures the essence of the $I^{(2)}$CARS process in a more tangible and presumably more easily understandable way. So, the goal of this section is to build such a model that consistently brings one to the same conclusions as the mathematical treatment.

We know that the (narrowband detected) $I^{(2)}$CARS interferogram is dominated by the terms of the form[20,22,23,27−29]

$$I \sim e^{-2\gamma_{mg}|\tau|}\left[\frac{\cos\Delta_A\tau}{2\gamma_{mg}} + \frac{\sin\Delta_A|\tau|}{\Delta_A}\right] \qquad (17)$$

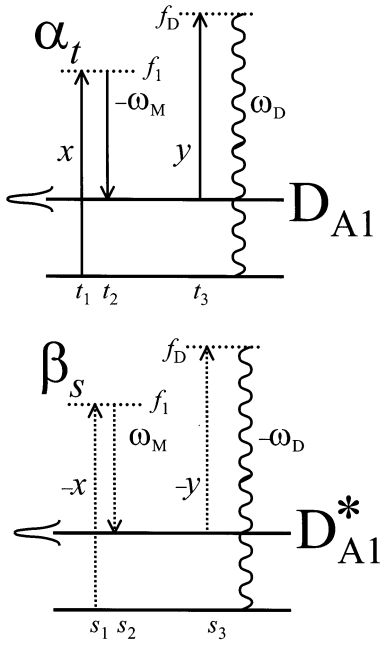

Figure 10. Rationalization of the cosine term in mathematical formula for $I^{(2)}$CARS. See text for a detailed discussion. Dashed horizontal lines represent virtual states that collapse exceedingly rapidly and thus result in the "elastic field-connection."

The complete set of WMEL diagrams for the $I^{(2)}$CARS signal are shown elsewhere,[28] and the τ-dependent FTC diagrams are the same as those in diagrams Ia−Id in Figure 8. For brevity, the discussion will be limited to D_{A1} and D^*_{A1} of Figure 6. The arguments may be easily extended to the other diagrams. Since γ_{mg} is the only decay rate constant to be discussed in the remainder of the chapter, we drop the subscripts for convenience ($\gamma \equiv \gamma_{mg}$).

A. Rationalization of the Cosine Term. The cosine term in expression (17) is associated with the uncrossed FTC diagrams (Ia and Ib in Figure 8). On any given chromophore α_t with the associated WMEL diagram D_{A1} of Figure 10, the first action by the noisy field at some frequency x is limited to within the bandwidth of the noisy light spectrum J, all frequencies of which are represented across the ensemble of chromophores. However, those members of the ensemble for which the intervening frequency x satisfies $(\omega_{\mathbf{M}} + \omega_R - \gamma/2) < x < (\omega_{\mathbf{M}} + \omega_R + \gamma/2)$ give an enhanced contribution to the eventual production of the fourth wave. It is for just these x that the subsequent action of the monochromatic field $\omega_{\mathbf{M}}$ can reach the real state m (bandwidth γ) and enjoy a Raman resonance (*stage1 filter*). We shall focus on these Raman resonant chromophores. The first action of x, Raman resonance limited to roughly γ, reaches a virtual state f_1. Because f_1 collapses exceedingly rapidly, the monochromatic field $\omega_{\mathbf{M}}$ must then act "instantaneously;" i.e., on a time scale much faster then any chromophore−bath interaction. This is represented in the WMEL diagram of Figure 10 as the arrow tail of $\omega_{\mathbf{M}}$ starting exactly at the same virtual state f_1 at the head of the x arrow. This will be referred to as an *elastic field-connection*. Now, a particular frequency y selected from the noisy light may act any time during the decay of the vibrational coherence. This is on a time scale where energy may be exchanged (inelastic) with the bath, so the tail of y may start anywhere within a spread γ about the center Bohr frequency ω_R (inelastic field-connection), but it must reach the sharp virtual state f_D set by the exact detector setting $\bar{\omega}_D$; otherwise, the induced polarization will launch a fourth wave at a frequency $\omega_s \neq \bar{\omega}_D$ which will not reach the detector (this is the action of the *stage2 filter*). So, of the entire noisy spectrum J, y is limited to $(\bar{\omega}_D - \omega_R - \gamma/2) < y < (\bar{\omega}_D - \omega_R + \gamma/2)$. Thus, the energy conservation condition is $x + y + \Delta E_{bath} = \omega_{\mathbf{M}} + \bar{\omega}_D$, where ΔE_{bath} is the energy exchanged with the bath and may be as large as roughly 2γ. At every detected frequency $\bar{\omega}_D$, there are two degrees of freedom: x (or y) and ΔE_{bath}. The total range of frequencies across the ensemble for resonant diagram D_{A1} in Figure 10 is roughly 2γ [a bandwidth of γ is available to both x and y $(\gamma + \gamma = 2\gamma)$].

Now, because of color locking, only a very specific second (conjugate) chromophore β_s may partner with α_t at the quadrature level. Here, the first intervention must be exactly the same x (acting conjugately) as that in D_{A1}. Again, $\omega_{\mathbf{M}}$ (acting conjugately) acts on β_s "instantaneously" (elastic field-connection) from virtual state f_1 and resonance is automatically achieved (given that resonance was achieved on α_t). The same y (now acting conjugately at *stage2*) then acts to always reach the sharp detector setting. In this example, there is never any $x-y$ conflict, so $x \simeq (\omega_{\mathbf{M}} + \omega_R)$ and $y \simeq (\bar{\omega}_D - \omega_R)$ always. A $x-y$ conflict refers to the case where x and y both enjoy resonance on α_t (β_s) but neither do on the conjugate chromophore β_s (α_t). The $\cos\Delta_A\tau$ is rationalized as before: a difference beating of filter functions. Since ΔE_{bath} must be the same for D^*_{A1} as that for D_{A1}, no additional spread is introduced, so the cosine term multiplied by the factor of $^1/_2\gamma$ accounts for the integration over the overall spread (in the cosine term) of the bichromophoric contribution across the ensemble. The 2γ decay with τ is a result of indirect correlation.

B. Rationalization of the Sine Term. The sine term in expression (17) is associated with the crossed diagrams (Ic and Id of Figure 8). Without loss of generality, we may take the same situation for chromophore α_t as when rationalizing the cosine term: a x filter exists at *stage1* and a y filter exists at *stage2*. Now, for crossed FTC diagrams, this α_t is paired with a conjugate partner (β_s) chromophore at the quadrature level whose first intervention (*stage1*) must be exactly y (because of color locking) reaching virtual state f_2. In general $x \neq y$, and the subsequent "instantaneous" action of $\omega_{\mathbf{M}}$ cannot achieve a Raman resonance as it did for uncrossed diagrams (compare D^*_{A1} of Figure 10 and D^*_{A1} of Figure 11) since y is not the same color (to within γ) selected by the *stage1 filter*. If resonance is not achieved, only a virtual state f_3 is reached (as opposed to the real state m for the uncrossed FTC diagram case) in *stage1* and, in the third step on β_s, x appears (color-locked from *stage1* on α_t) and is now elastically field-connected to $\omega_{\mathbf{M}}$. It must act instantaneously from virtual state f_3 as opposed to the case for the uncrossed diagrams, in which x can always act inelastically during the decay of the vibrational coherence. Again, resonance exists after *stage1* on α_t but not on β_s for the crossed FTC diagrams; it exists after *stage1* on both α_t and β_s for the uncrossed diagrams. This loss of inelastic field-connection between the *stage1* and *stage2* sharply tightens the conservation of energy constraint to $(x + y) = (\omega_{\mathbf{M}} + \bar{\omega}_D)$. The influence of the bath is eliminated and there is a loss of a degree of freedom (ΔE_{bath}). The diagrams have zero spread across the ensemble. The consequent sine behavior of the interferogram can be rationalized in a manner similar to that for electronically resonant versus electronically nonresonant impulsive Raman scattering. It is also similar to the resonant−nonresonant $I^{(2)}$-CARS cross terms in (resonant) solute−(nonresonant) solvent systems.[20,22,23,27−29] They both have terms exhibiting pure sine behavior. In each of these cases, it is argued that there is a factor of i distinction between the nonresonant and resonant limits of a given density matrix element. That is, in the nonresonant limit,

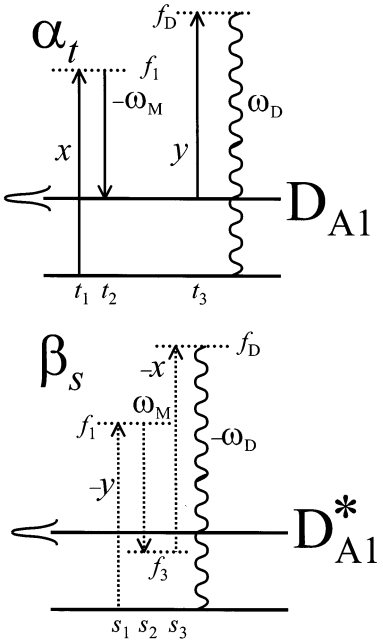

Figure 11. Rationalization of the sine term in mathematical formula for $I^{(2)}$CARS. See text for a detailed discussion. Dashed horizontal lines represent virtual states that collapse exceedingly rapidly and thus result in the "elastic field-connection."

one of the energy denominators is approximately purely real, but in the resonant limit this same energy denominator is approximately purely imaginary; hence, the two limits differ by an imaginary constant and are out of phase by i (or $\pi/2$). For our case (with $x \neq y$), D_{A1} (on α_t) is fully resonant (now with spread zero from the stronger energy conservation constraint) and D^*_{A1} (on β_s) is nonresonant. So, we have a necessarily resonant−nonresonant situation for the crossed FTC diagrams in contrast to the resonant-resonant case for the uncrossed FTC diagrams. Thus, these two cases differ by a factor of i; thus, the crossed FTC diagrams are phase-shifted by $\pi/2$ with respect to the (cosine-like) uncrossed diagrams. They are therefore sine-like. Here, because of the $x-y$ conflict regarding resonance, the sine terms are weaker than the cosine terms.

It should be noted that, for the crossed FTC diagrams, one chromophore (α_t or β_s) locks onto a perfect resonance after *stage1* and the other is fully nonresonant rather then each being somewhat off resonance. We need not (to a good approximation) consider the case where each chromophore is somewhat off resonance.[64] Only one parameter Δ_A is needed to characterize the detuning from resonance for

$$(y - \omega_{\mathbf{M}} - \omega_R) = (\bar{\omega}_D - x - \omega_R) = \Delta_A \equiv (\bar{\omega}_D - \omega_{\mathbf{M}} - 2\omega_R) \quad (18)$$

[see β_s (D^*_{A1}) in Figure 11]. That one chromophore is always in perfect resonance while the other is fully off resonance in the crossed FTC diagram case is simply a limit of an optimization problem.[64]

The above phase shift argument works well for the $x \neq y$ case, but it breaks down when $x \rightarrow y$ (small detuning: $\Delta_A \rightarrow 0$). At first glance, it appears that the conservation of overall energy constraint should be relaxed when $x \simeq y$ since y is no longer forced to launch from a virtual state (there now is no $x-y$ conflict), and hence, the sine contribution should become cosine-like as $\Delta_A \rightarrow 0$. However, the more precise mathematical treatment shows[20,22,23,27−29] that the sine term appears for all x

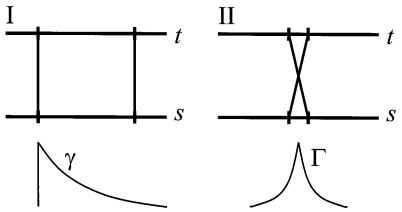

Figure 12. Topological constraints of the FTC diagrams force a $\pi/2$ phase shift between the cosine term arising from the uncrossed FTC diagram and the sine term arising from the crossed FTC diagram. See text for more details.

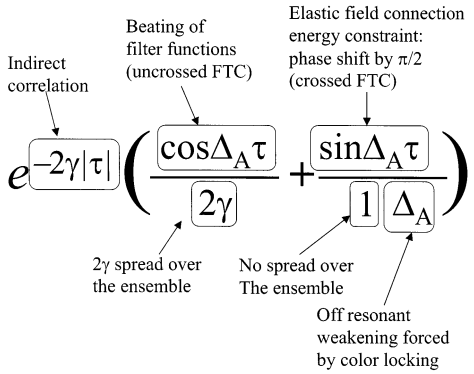

Figure 13. The mathematical anatomy of the $I^{(2)}$CARS signal and the physical concepts that explain the various factors in the expression.

(even when $\Delta_A \rightarrow 0$), so there must be an additional constraint that removes the ΔE_{bath} degree of freedom. This constraint can most easily be seen if one takes $\tau \simeq 0$ and goes to the white light limit for the noisy source ($\tau_c \rightarrow 0$). Under these conditions, it is easy to see that the uncrossed (diagram I in Figure 12) and crossed (diagram II in Figure 12) FTC diagrams are very different in terms of accumulation and more importantly with regard to intervention times. Diagram I illustrates the fact that the two tick marks on the s and t time lines may have nonzero separation (y need not act instantly after $\omega_{\mathbf{M}}$). Conversely, diagram II enjoys no such separation of the light interventions and again y is forced to act with elastic field-connection with $\omega_{\mathbf{M}}$ even when on resonance. In a sense, diagram II is not allowed to feel the resonance. That is, the crossed nature of the pair correlators forces the instantaneous action of *stage1* and *stage2* . The resonance cannot be explored on one of the two chromophores (even though $x = y$). Thus, the strict energy conservation condition is maintained for all $x - y$, even those such that $x \simeq y$. As a result, the sine behavior is likewise maintained for all $x - y$ not just the in case when $x \neq y$. The elastic field-connection condition leads to no spread over the ensemble and hence no $1/2\gamma$ factor. Furthermore, the contribution must be weaker (relative to the cosine term) by the degree of nonresonance Δ_A, giving the $1/\Delta_A$ factor. This crossed FTC diagram continues to allow for indirect correlation and hence to the $e^{-2\gamma|\tau|}$ behavior. Figure 13 shows the anatomy of the expression for the $I^{(2)}$CARS interferogram with the corresponding physical pictures as indicated.

V. Conclusion

The goal of this paper was to set forth several physical concepts which have proven to be of substantial aid in the understanding of the underlying physical mechanisms of noisy light spectroscopy. The technique of factorized time correlation diagram analysis and the WMEL diagrams with their ties to the previous mathematical treatment of the noisy light problem

served as a basis for these physical notions. We saw that each concept manifests itself as an observable characteristic of a particular noisy light process. Examples were given to add concreteness the general discussions of the physical concepts. $I^{(2)}$CARS served as a particularly useful example. It is not the role of these concepts developed here to take the place of further mathematical treatment of noisy light−matter interaction, but it is hoped that this ideas will serve to guide future investigation on both the experimental and theoretical fronts.

Acknowledgment. The author thanks Paul Houston for the invitation to submit a manuscript as a contribution to this special issue. The author is forever grateful to professor A.C. Albrecht and will miss him deeply.

References and Notes

(1) Morita, N.; Yajima, T. *Phys. Rev. A* **1984**, *30*, 2525.
(2) Nakatsuka, N.; Tomita, M.; Fujiwara, M.; Asaka, S. *Phys. Rev. A* **1984**, *29*, 2286.
(3) Beach, R.; Hartmann, S. R. *Phys. Rev. Lett.* **1984**, *53*, 663.
(4) Yang, T.-S.; Zhang, R.; Myers, A. B. *J. Chem. Phys.* **1994**, *100*, 8573.
(5) Zhang, Y.; Moshary, F.; Hartmann, S. R. *Laser Phys.* **1995**, *5*, 676.
(6) Kummrow, A.; Lau, A. *Appl. Phys. B* **1996**, *63*, 209.
(7) Rao, D. N.; Rao, S. V.; Aranda, F. J.; Rao, D. V. G. L. N.; Nakashima, M.; Akkara, J. A. *J. Opt. Soc. B* **1997**, *14*, 2710.
(8) Rao, S. V.; Rao, D. N. *Chem. Phys. Lett.* **1998**, *283*, 227.
(9) Kozich, V. P.; de Menezes, L. S.; de Araujo, C. B. *J. Opt. Soc. B* **2000**, *17*, 973.
(10) Kozich, V. P.; de Menezes, L. S.; de Araujo, C. B. *Opt. Lett.* **2001**, *26*, 262.
(11) Rao, S. V.; Naga Srinivas, N. K. M.; Rao, D. N.; Giribabu, L.; Maiya, B. G.; Philip, R.; Kumar, G. R. *Opt. Commun.* **2001**, *192*, 123.
(12) Kobayashi, T. *Adv. Chem. Phys*. **1994**, *85*, 55.
(13) Stimson, M. J.; Ulness, D. J.; Kirkwood, J. C.; Boutis G.; Albrecht, A. C. *J. Opt. Soc. B* **1998**, *15*, 505.
(14) DeMott, D. C.; Ulness, D. J.; Albrecht, A. C. *Phys. Rev. A* **1997**, *55*, 761.
(15) Ulness, D. J.; Albrecht, A. C. *Phys. Rev. A* **1996**, *53*, 1081.
(16) Ulness, D. J.; Albrecht, A. C. *J. Raman Spectrosc.* **1997**, *28*, 571.
(17) Ulness, D. J.; Kirkwood, J. C.; Stimson, M. J.; Albrecht, A. C. *J. Chem. Phys.* **1997**, *107*, 7127.
(18) Kirkwood, J. C.; Ulness, D. J.; Stimson, M. J.; Albrecht, A. C. *Phys. Rev. A* **1998**, *58*, 4910.
(19) Hattori, T. Teraski, A.; Kobayashi, T. *Phys. Rev. A* **1987**, *35*, 715.
(20) Dugan, M. A.; Melinger, J. S.; Albrecht, A. C. *Chem. Phys. Lett.* **1988**, *147*, 411.
(21) Wynne, K.; Müller, M.; Van Voorst, J. D. W. *Phys. Rev. A*, **1990**, *41*, 6361.
(22) Dugan, M. A.; Albrecht, A. C. *Phys. Rev. A* **1991**, *43*, 3877.
(23) Dugan, M. A.; Albrecht, A. C. *Phys. Rev. A* **1991**, *43*, 3922.
(24) Schaertel, S. A.; Albrecht, A. C. *J. Raman Spectrosc*. **1994**, *25*, 545.
(25) Lau, A.; Kummrow, A.; Pfeiffer, M.; Woggon, S. *J. Raman Spectrosc.* **1994**, *25*, 607.
(26) Okamoto, H.; Nakabayashi, T.; Tasumi, M. *J. Raman Spectrosc*. **1994**, *25*, 631.
(27) Schaertel, S. A.; Albrecht, A. C.; Lau, A.; Kummrow, A. *Appl. Phys. B* **1994**, *59*, 377.
(28) Schaertel, S. A.; Lee, D.; Albrecht, A. C. *J. Raman Spectrosc.* **1995**, *26*, 889.
(29) Stimson, M. J.; Ulness, D. J.; Albrecht, A. C. *Chem. Phys. Lett.* **1996**, *263*, 185.
(30) Kozich, V. P.; Lau, A.; Kummrow, A. *J. Raman Spectrosc*. **1999**, *30*, 473.
(31) Ulness, D. J.; Stimson, M. J.; Kirkwood, J. C.; Albrecht, A. C. *J. Phys. Chem.* **1997**, *101*, 4587.
(32) Ulness, D. J.; Stimson, M. J.; Kirkwood, J. C.; Albrecht, A. C. *J. Raman Spectrosc.* **1997**, *28*, 917.
(33) Ulness, D. J.; Stimson, M. J.; Kirkwood, J. C.; Albrecht, A. C. *Laser Chem.* **1999**, *19*, 11.
(34) Ulness, D. J.; Stimson, M. J.; Albrecht, A. C. *Chem. Phys.* **1997**, *222*, 17.
(35) Ulness, D. J.; Kirkwood, J. C.; Stimson, M. J.; Albrecht, A. C. *Asian J. Phys.* **1999**, *7*, 405.
(36) Ulness, D. J.; Stimson, M. J.; Albrecht, A. C. *J. Raman Spectrosc.* **1997**, *28*, 579.
(37) Kurokawa, K.; Hattori, T.; Kobayashi, T. *Phys. Rev. A* **1987**, *36*, 1298.
(38) Misawa, K.; Hattori, T.; Kobayashi, T. *Opt. Lett.* **1989**, *14*, 453.
(39) Vodchits, A. I.; Kozich, V. P.; Kontsevoi, B. L. *Opt. Spectrosc.* **1991**, *70*, 516.
(40) Apanasevich, P. A.; Vodchits, A. I.; Kozich, V. P. *Opt. Spectrosc.* **1993**, *74*, 559.
(41) Al-ghamdi, A. A. *App. Opt.* **2001**, *40*, 2485.
(42) Albrecht, A. C.; Smith, S. P.; Tan, D.; Schaertel, S. A.; DeMott, D. C. *Laser Phys*. **1995**, *5*, 667.
(43) Pfeiffer, M.; Lau, A. *J. Chem. Phys.* **1998**, *108*, 4159.
(44) Kirkwood, J. C.; Ulness, D. J.; Albrecht, A. C. *J. Chem. Phys.* **1998**, *108*, 9425.
(45) Kirkwood, J. C.; Ulness, D. J.; Stimson, M. J.; Albrecht, A. C. *Chem. Phys. Lett.* **1998**, *293*, 417.
(46) Lau, A.; Pfeiffer, M.; Kummrow, A. *Chem. Phys. Lett.* **1996**, *263*, 435.
(47) Lau, A.; Pfeiffer, M.; Tschirschwitz, F. *J. Chem. Phys.* **1998**, *108*, 4173.
(48) Kirkwood, J. C.; Ulness, D. J.; Albrecht, A. C. *J. Chem. Phys.* **1999**, *111*, 253.
(49) Kirkwood, J. C.; Ulness, D. J.; Albrecht, A. C. *J. Chem. Phys.* **1999**, *111*, 272.
(50) Kirkwood, J. C.; Albrecht, A. C. *J. Raman Spectrosc.* **2000**, *31*, 107.
(51) Dawlaty, J. M.; Ulness, D. J. *J. Raman Spectrosc.* **2001**, *32*, 211.
(52) Kirkwood, J. C.; Albrecht, A. C. *Phys. Rev. A* **2000**, *61*, 033802.
(53) Kirkwood, J. C.; Albrecht, A. C. *Phys. Rev. A* **2000**, *61*, 043803.
(54) Mukamel, S. *Principles of Nonlinear Optical Spectroscopy*, Oxford University Press: New York, 1995.
(55) Hanamura, E. *Solid State Commun*. **1981**, *51*, 9.
(56) Hanamura, E.; Mukamel, S. *Phys. Rev. A* **1986**, *33*, 1099.
(57) Mandel, L.; Wolf, E *Optical Coherence and Quantum Optics*; Cambridge University Press: New York, 1995.
(58) Kirkwood, J. C.; Ulness, D. J.; Albrecht, A. C. *J. Phys. Chem. A* **2000**, *104*, 4167.
(59) Yee, T. K.; Gustufson, T. K. *Phys. Rev. A* **1978**, *18*, 1597.
(60) Lee, D.; Albrecht, A. C. In *Advances in Infrared Spectroscopy*; Clark, R. J., Hester, R. E., Eds.; Wiley-Heyden: New York, 1985.
(61) Roman, P.; Wolf, E. *Nouvo Cimento* **1960**, *17*, 462.
(62) Kummrow, A. Lau, A and Lenz, K. *Phys. Rev. A* **1997**, *55*, 2310.
(63) Biebighauser, D. P.; Turner, D. B.; Ulness, D. J. *Phys. Rev. E* **2002**, *65*, 026142.
(64) Ulness, D. J. Ph.D. Thesis, Cornell University, Ithaca, NY, 1996.